Random Field Driven Spatial Complexity at the Mott Transition in VO_{2}

Shuo Liu, B. Phillabaum, E. W. Carlson, K. A. Dahmen, N. S. Vidhyadhiraja, M. M. Qazilbash, and D. N. Basov

Phys. Rev. Lett. **116**, 036401 — Published 22 January 2016

DOI: 10.1103/PhysRevLett.116.036401

Random Field Driven Spatial Complexity at the Mott Transition in VO_2

Shuo Liu,[1,*] B. Phillabaum,[1] E. W. Carlson,[1] K. A. Dahmen,[2]
N. S. Vidhyadhiraja,[3] M. M. Qazilbash,[4] and D. N. Basov[5]

[1]*Department of Physics, Purdue University, West Lafayette, IN 47907, USA*
[2]*Department of Physics, University of Illinois, Urbana-Champaign, IL 61801, USA*
[3]*Jawaharlal Nehru Centre for Advanced Scientific Research, Bangalore 560064, India*
[4]*Department of Physics, College of William and Mary, Williamsburg, VA 23187, USA*
[5]*Department of Physics, University of California-San Diego, La Jolla, CA 92093, USA*

(Dated: December 3, 2015)

We report the first application of critical cluster techniques to the Mott metal-insulator transition in vanadium dioxide. We show that the geometric universal properties of the metallic and insulating puddles observed by scanning near-field infrared microscopy are consistent with the system passing near criticality of the random field Ising model as temperature is varied. The resulting large barriers to equilibrium may be the source of the unusually robust hysteresis phenomena associated with the metal-insulator transition in this system.

The Mott metal-insulator transition in VO_2 has the potential to produce disruptive technologies, such as memristors, memory capacitors, ultrafast switches, and possibly even neuromorphic circuits [1]. Yet despite decades of research into VO_2, the nature of the phase transition, and in particular the broad hysteretic behavior accompanying it, is not yet understood. In V_2O_3, there is a first order phase transition whose critical endpoint was argued to be in the universality class of the clean three-dimensional (3D) Ising model [2–4]. In VO_2, the resistance avalanches observed in Ref. 5 were interpreted in terms of the universality class of uncorrelated percolation [5]. Here, we argue that the first order metal-insulator transition in VO_2 is also near a critical endpoint which can be reached by tuning disorder. Using quantitative cluster techniques, we argue that the critical endpoint is in the universality class of the random field Ising model, which is well-known for nonequilibrium effects such as broad hysteresis.

As shown in Fig. 1, scanning near-field infrared microscopy (SNIM) on VO_2 [6] reveals that the transition from the low temperature insulating phase to the high temperature metallic phase is accompanied by the complex pattern formation expected in a disordered correlated electronic system, in which spatial fluctuations in disorder nucleate different phases [7]. Using recently developed cluster techniques [8], we show below that the cluster statistics are power law over 2.5 decades, consistent with proximity to a critical endpoint of the first order phase transition. In fact it has recently been shown that the hysteretic behavior in VO_2 can be tuned through a critical endpoint via doping [9, 10]. Fig. 2(a) shows the coexistence region, inferred by taking the maximum slope of resistivity vs. temperature curves as a function of Nb doping from Fig. 3(b) of Ref. 9.

We analyze the SNIM images in Fig. 1 under the assumption of proximity to this critical endpoint. In the original SNIM data images [6], we assign Ising variable [11] $\sigma = 1$ (metallic) or -1 (insulating) to each coarse-grained region [2–4, 12, 13]. Our results are robust against changes of as much as 15% in the threshold amplitude a_{th} used to identify metallic regions (those with scattering amplitude $a > a_{th}$) and insulating regions (with $a \leq a_{th}$), and in the main text we show results with the representative value of $a_{th} = 2.5$. (See SI.) We furthermore incorporate disorder into the model:

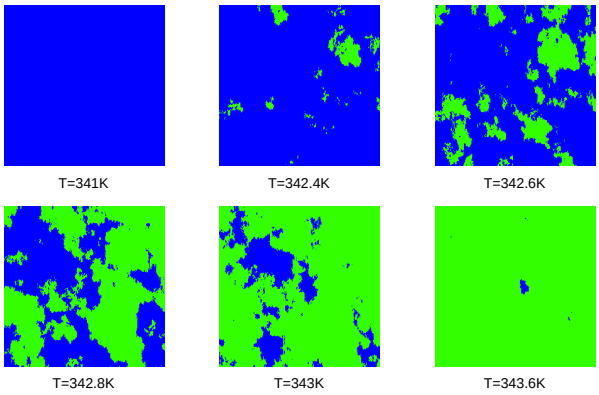

FIG. 1. Scanning Near-field Infrared Microscopy on VO_2 as temperature is increased through the Mott metal-insulator transition regime, over the same $4\mu m \times 4\mu m$ sample area. These figures are Ising-mapped from the original SNIM images in Ref. [6] with threshold scattering amplitude $a_{th} = 2.5$. The metallic regions, colored green, give higher near-field scattering amplitude, $a > a_{th}$, compared with the insulating regions with $a \leq a_{th}$, colored blue.

$$H = -\sum_{\langle ij\rangle_{\parallel}}^{\infty}(J+\delta J_{ij})\sigma_i\sigma_j - \sum_{\langle ij\rangle_{\perp}}^{L_z}(J+\delta J_{ij})\sigma_i\sigma_j - \sum_i (h+h_i)\sigma_i \ , \quad (1)$$

where the sum runs over the coarse-grained regions (sites) consisting of a cubic lattice, chosen with spacing at least as small as the resolution of the images to be studied.

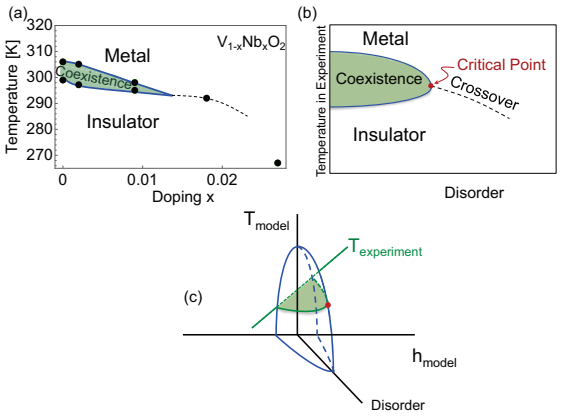

FIG. 2. (a) Metal-insulator coexistence region terminating in disorder-induced critical endpoint, inferred from Nishikawa *et al.* [9], Fig. 3(b). Schematic theoretical phase diagrams showing coexistence region (in green) (b) in the experimental temperature *vs.* disorder strength plane; (c) with respect to model temperature T_{model}, effective field h_{model}, and disorder strength.

The tendency for neighboring regions to be of like character is modeled as a nearest neighbor ferromagnetic interaction $J > 0$. Because the data considered is that of a thin film, the sum over Ising variables in the plane of the film (denoted by $\|$) extends to infinity, but the sum over Ising variables perpendicular to the film surface(denoted by $\perp$) is finite, confined by the film thickness L_z.

At the order parameter level, there are two broad classes of disorder: local energy density disorder (which we incorporate as random bond disorder), and random field disorder [14]. In Eqn. 1, random bond disorder is included through the term δJ_{ij}, and h_i represents random field disorder, which is chosen from a gaussian probability distribution centered about zero, with variance R. R is often called the disorder parameter or just disorder. Because the field h represents a generalized external field which couples with the local Ising variables, tuning temperature in experiment also sweeps the generalized field h in the model, as schematically illustrated in Fig. 2(c).

Using the mapping to Ising variables (Fig. 1), we track the geometric clusters, defined as connected sets of nearest neighbor sites (pixels) with the same color. We then use the statistics of the sizes and shapes of these clusters to identify the cause of the pattern formation. In comparing the spatial complexity revealed in the SNIM data to theory, there are 7 fixed points of Eqn. 1 to consider [8]. In the two-dimensional case, these consist of the clean Ising model (C-2D), uncorrelated percolation (P-2D), and the random field Ising model (RF-2D). Note that random bond disorder is irrelevant in the renormalization group sense in 2D, and the phase transition is therefore governed by clean Ising model exponents (C-2D). In the three-dimensional case, the possible fixed points are the clean Ising model (C-3D), uncorrelated

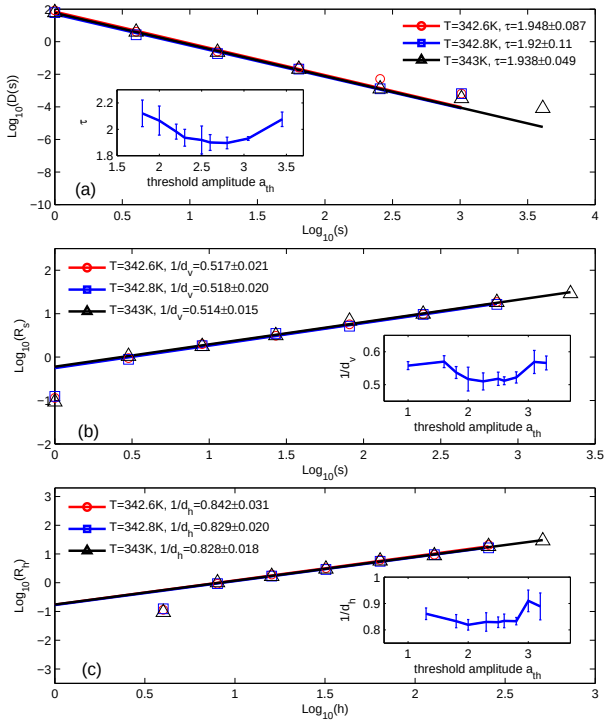

FIG. 3. Power law fits of internal clusters from the VO_2 SNIM image datasets with threshold scattering amplitude $a_{th} = 2.5$ for (a) $D(s) \propto s^{-\tau}$, (b) $R_s \propto s^{1/d_v}$, and (c) $R_h \propto h^{1/d_h}$, at three intermediate temperatures $T = 342.6K$, $T = 342.8K$, and $T = 343K$. The insets show the extracted τ, $1/d_v$, and $1/d_h$ (with error bars) as a function of a_{th} at T=342.8K.

percolation (P-3D), the random bond Ising model (RB-3D), and the random field Ising model (RF-3D). In the case of a film, as the Ising correlation volume grows to exceed the film thickness, the critical exponents evident in the cluster geometries should drift from 3D to 2D critical behavior.

From the SNIM images, we extract three critical exponents from the self-similarity of the geometric clusters near certain critical points: The Fisher exponent τ characterizes the cluster-size distribution $D(s) \propto s^{-\tau}$. The volume fractal dimension d_v and the hull fractal dimension d_h characterize the fractal nature of cluster sizes s and hulls h. For the cluster sizes, $s \propto R_s^{d_v}$, where R_s is the radius of gyration of the cluster [15]. For the cluster surfaces, $h \propto R_h^{d_h}$, where R_h refers to the radius of gyration of *all* the sites enclosed by the hull, including any subclusters inside. To reduce noise due to the finite field of view (FOV), we apply logarithmic binning [16] throughout this Letter. The values of critical exponents are obtained by taking the discrete logarithmic derivative (DLD) [17]. We restrict our analysis to internal clusters, i.e., clusters which do not intersect the boundary of the FOV, in order to mitigate finite FOV effects which skew the estimated values of the extracted exponents [18, 19].

The main panels in Fig. 3 show explicitly the power law

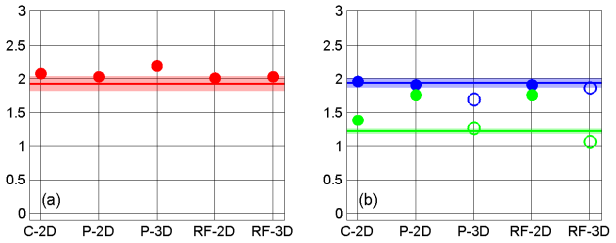

FIG. 4. Exponent comparison charts. (a) Critical exponent τ. (b) Critical exponents d_v (blue) and d_h (green). The horizontal lines are our extracted exponents from the SNIM images, with the shaded regions being their error bars. The circles represent theoretical values [8, 20] for the fixed points of Eqn. 1. When comparing with 3D models, we have to use the effective values of d_v and d_h corresponding to taking 2D cross sections of the clusters embedded in 3D, *i.e.* $d_v^* = 2d_v/3$ and $d_h^* = d_h/2$ [8]. These effective values are represented by the open circles.

fits of these critical cluster exponents at three intermediate temperatures (which have enough clusters for good statistics) with threshold scattering amplitude $a_{th} = 2.5$. For τ, two decades of scaling are evident, and the remaining points fall off the scaling regime. This phenomenon is consistent with the use of internal clusters, and τ extracted in this way is less affected by the finite size window effects, since within a cutoff in the decades of scaling $D(s)$ of internal clusters shares the same power law slope as the full system [19]. For the fractal dimensions, with the first bin (which contains $s = 1$ clusters) excluded [20], robust power law scaling extends over multiple decades, encompassing the entire FOV. The robust power law behaviors, as well as the fact that the values of the cluster exponents are the same within error bars for different intermediate temperatures, corroborates the idea that the system is near a critical end point of the Mott transition. The insets of Fig. 3 show our extracted τ, d_v, and d_h using different a_{th} at the representative temperature $T = 342.8K$ which is closest to criticality, and within error bars these critical exponents are robust against changes in threshold amplitude within a broad stable region around $a_{th} = 2.5$, consistent with that given by the definition in Ref. [6]. This independence of results with respect to microscopic details also reflects universal behavior near criticality. Using $a_{th} = 2.5$ and T=342.8K as representative conditions, we have $\tau = 1.92 \pm 0.11$, $d_v = 1.93 \pm 0.07$, and $d_h = 1.21 \pm 0.03$ for the spatially complex clusters near the critical end point of the Mott transition in VO_2.

Before comparing the data-derived critical exponents to their known theoretical values for the fixed points of Eqn. 1, the C-3D and RB-3D fixed points can be ruled out *a priori*. Since geometric clusters are not fractal at these two fixed points [21–23], they cannot be the cause of the robust power law behavior observed in Figs. 3. Geometric clusters do exhibit fractal behavior at the remaining five fixed points (C-2D, RF-2D, RF-3D, P-2D, and P-3D) [15, 17, 21, 24]. Within this set of candidate fixed points, there are two possible dimensional crossovers, which are (1) between RF-2D and RF-3D in the presence of random field disorder, and (2) between C-2D and the 3D percolation points $T_p < T_c$ in the clean and random bond Ising models, where the exponents should follow those of uncorrelated percolation, P-3D [23, 25, 26].

As shown in Fig. 4, the values of τ and d_v resulting from our analysis are fairly close to all fixed points except P-3D, which can thus be ruled out as an origin of the power law behavior. Unlike τ and d_v, the theoretical values of d_h vary significantly for the various fixed points. We see immediately from Fig. 4(b) that the theoretical values of d_h at P-2D and RF-2D are abruptly inconsistent with the data. Only two candidate fixed points remain (C-2D and RF-3D), but in Fig. 4(b), both show about a 13% discrepancy between the data and the theoretical model for the value of d_h, which is significantly larger than the typical error of about 3% of the exponents extracted from the data.

We turn then to the possibility of dimensional crossovers. For the candidate dimensional crossover from P-3D to C-2D, the value of d_v is much closer to C-2D than to P-3D, consistent with the geometric clusters being near their 2D limit, whereas the value of d_h is much closer to P-3D than to C-2D, indicating that the geometric clusters are near their 3D limit. This inconsistency strongly argues against the P-3D to C-2D dimensional crossover as the origin of the power law behavior.

The other candidate dimensional crossover is from RF-3D to RF-2D. The exponent comparisons show no inconsistency with this explanation, since within error bars τ and d_v match the RF-2D to RF-3D crossover regime, and d_h is also consistent with this dimensional crossover. Therefore, the random field Ising universality class best describes the critical behavior of the Mott transition in the VO_2 thin film, revealing the key role played by disorder effects in these systems. Observations at longer length scales can be used to test this hypothesis: if our identification is correct, then the values of all exponents should drift toward RF-2D with larger fields of view in a film geometry such as the present one.

In order to further test whether the spatial complexity is driven by random field effects, we also analyze the avalanches which, in the context of the VO_2 experiment, are defined as the difference between Ising maps between two neighboring temperatures. Figure 5 shows the power law fits of the internal avalanches with threshold $a_{th} = 2.5$ for the data-extracted τ', d'_v, and d'_h, using the same techniques as for the clusters in Fig. 3. The prime symbol is used to denote that these exponents are for avalanches. Similar to their cluster counterparts, the cut-off for internal avalanche scaling for τ' is about 1.5 to 2 decades of scaling, and d'_v and d'_h show multiple decades

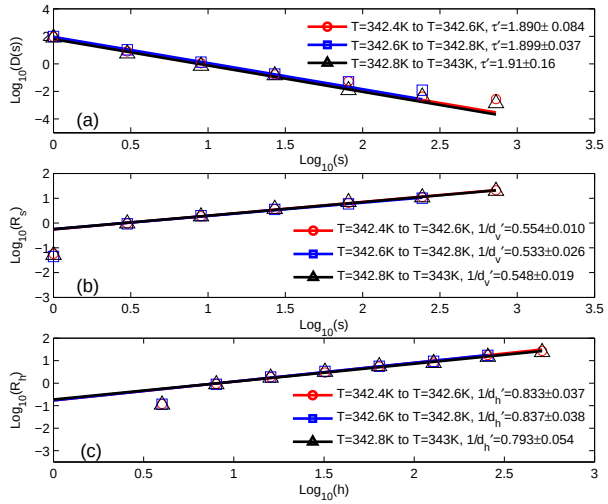

FIG. 5. Power law fits of internal avalanches from the VO_2 SNIM image datasets with threshold scattering amplitude $a_{th} = 2.5$ for (a) $D(s) \propto s^{-\tau'}$, (b) $R_s \propto s^{1/d'_v}$, and (c) $R_h \propto h^{1/d'_h}$, at three intermediate intervals with $\Delta T = 0.2K$ through the Mott transition

.

of power law scaling behavior. For different intervals, the extracted critical avalanche exponents are consistent with each other within error bars. This data-extracted robust universal power law scaling of avalanches provides further evidence that the random field universality is underlying the complex pattern formation at the Mott transition in the VO_2 thin film, since non-trivial scaling behavior of avalanches is characteristic of random field physics.

Since the avalanches are taken from the finite interval between scanned images, the data-extracted τ' in our context characterizes the scaling of the field integrated avalanche size distribution $D_{int}(s)$ near criticality. The corresponding exponent is reported to be 2.03 ± 0.03 for RF-3D [18, 27, 28] and 1.3 ± 0.1 for RF-2D [29], and the corresponding data-extracted one from Fig. 5(a) lies in between, consistent with the conclusion of a dimensional crossover from RF-3D to RF-2D. With d'_v and d'_h only reported for RF-3D [28], our data-extracted fractal dimensions (Fig. 5(b) and 5(c)) could not be directly compared with the theoretical ones for the RF-3D to RF-2D crossover. However, within error bars, d'_v and d'_h extracted from avalanches have the same values as d_v and d_h extracted from clusters (Fig. 3(b) and 3(c)). This is consistent with Ref. [28], which shows that clusters and avalanches have the same exponents in the random field Ising model (RFIM).

The dominance of random field disorder is quite reasonable in a real physical system, arising from defects and impurities in the crystal structure; randomness in grain size, orientation, and boundary structure; and imperfections in the substrate. In the case of the sample under consideration, a likely source of random field effects is grain boundaries, as supported by our prior work showing that metallicity nucleates first near grain boundaries [30]. (See SI for a discussion of microscopic sources of disorder.) Several other characteristics of the data serve to corroborate the random field hypothesis. For example, as the Mott transition proceeds, metallic puddle formation occurs via nucleation and not just by front propagation [31], as shown in Fig. 1. In addition, as temperature increases through the transition (analogous here to sweeping the generalized field h of Eqn. 1), domains change from $\sigma = -1$ to $\sigma = +1$, but never revert. This no-passing rule is consistent with the random field universality class [28, 32, 33], indicating that the effects of quenched disorder dominate over thermal fluctuations. The dominance of quenched disorder over thermal effects is further corroborated by the reproducibility of the SNIM images, in that repeated near-field scans in the insulator-to-metal transition regime over the same sample area and at a fixed temperature show nearly identical patterns of metallic puddles in the insulating host [6, 34].

Finally, perhaps the most tell-tale sign of random field behavior in the data is the large width of the hysteresis in temperature, about $7.5K$ for temperature sweeps taking several minutes in a thin film [34, 35]. The extreme critical slowing down of the random field case means that barriers to equilibration grow much more severely as criticality is approached than the usual "critical slowing down" would predict. Hysteresis typically becomes long-lived near the critical endpoint of a first order phase transition, with the relaxation time t_{rel} diverging as a power law near the critical endpoint [36], $t_{rel} \propto \xi^z \propto |g - g_c|^{-\nu z}$, where g represents the relevant variable, whether temperature T or disorder strength R. ξ is the correlation length, ν is the exponent of the correlation length, and z is the dynamical exponent. Rather than a mere power law, barriers to equilibration grow exponentially near the RFIM critical endpoint [37], $t_{rel}^{\mathrm{RFIM}} \propto \exp[\xi^\theta] \propto \exp[1/|g - g_c|^{\nu\theta}]$, where θ is the "violation of hyperscaling" exponent. These exponentially large barriers to equilibration are consistent with the large width of hysteresis loops evident in this Mott metal-insulator transition. In addition, the large critical region typically associated with RFIM physics [18] is consistent with the wide range of parameters over which the broad hysteresis is observed.

In conclusion, by applying newly developed cluster techniques to SNIM data on VO_2, we have shown using six different critical exponents that the critical end point of the Mott transition is in the universality class of the random field Ising model. This finding reveals a delicate interplay between interaction and disorder in these systems. The random field Ising universality class has also recently been shown to account for the spatial structure of the locally oriented domains observed via scanning tunneling microscopy on cuprate superconduc-

tors [8, 38]. This further emphasizes the important role played by disorder in strongly correlated electron systems, and indicates that there may be universality to the spatial complexity [7, 39] observed in a wide variety of strongly correlated electron systems. The cluster techniques employed here can readily be applied to scanned images in the context of other materials and microscopy techniques for the study of universal behaviors underlying the spatial complexity.

We thank H. Aubin, J. Honig, and A. Zimmers for helpful conversations. S.L., B.P., and E.W.C. acknowledge support from NSF Grant No. DMR 11-06187. E.W.C. acknowledges receipt of an APS-IUSSTF Professorship Award, and thanks JNCASR for hospitality. K.A.D. acknowledges support from NSF Grant No. DMR 10-05209 and NSF Grant No. DMS 10-69224. N.S.V. acknowledges IUSSTF, JNCASR and Purdue University for funding the visitor exchange program. M.M.Q. acknowledges support from NSF Grant No. DMR 12-55156. D.N.B. acknowledges support from DOE-BES.

* liu305@purdue.edu

[1] Z. Yang, C. Ko, and S. Ramanathan, Annu. Rev. Mater. Res. **41**, 337 (2011).
[2] P. Limelette, A. Georges, D. Jérome, P. Wzietek, P. Metcalf, and J. M. Honig, Science **302**, 89 (2003).
[3] S. Papanikolaou, R. M. Fernandes, E. Fradkin, P. W. Phillips, J. Schmalian, and R. Sknepnek, Phys. Rev. Lett. **100**, 026408 (2008).
[4] F. Kagawa, K. Miyagawa, and K. Kanoda, Nature **436**, 534 (2005).
[5] A. Sharoni, J. G. Ramírez, and I. K. Schuller, Phys. Rev. Lett. **101**, 026404 (2008).
[6] M. M. Qazilbash, M. Brehm, B.-G. Chae, P.-C. Ho, G. O. Andreev, B.-J. Kim, S. J. Yun, A. V. Balatsky, M. B. Maple, F. Keilmann, H.-T. Kim, and D. N. Basov, Science **318**, 1750 (2007).
[7] E. Dagotto, Science **309**, 257 (2005).
[8] B. Phillabaum, E. W. Carlson, and K. A. Dahmen, Nat. Commun. **3**, 915 (2012).
[9] M. Nishikawa, T. Nakajima, T. Kumagai, T. Okutani, and T. Tsuchiya, Applied Surface Science **257**, 2643 (2011).
[10] K. Miyazaki, K. Shibuya, M. Suzuki, H. Wado, and A. Sawa, Japanese Journal of Applied Physics **53**, 071102 (2014).
[11] Note that while there is some spectroscopic difference between the infrared characteristics of the metallic puddles in the coexistence regime and the high temperature rutile metal [6], the coexistence regime is 2-phase and so it can be captured within an Ising description.
[12] C. Castellani, C. Di Castro, D. Feinberg, and J. Ranninger, Phys. Rev. Lett. **43**, 1957 (1979).
[13] G. Kotliar, E. Lange, and M. J. Rozenberg, Phys. Rev. Lett. **84**, 5180 (2000).
[14] J. Cardy, *Scaling and Renormalization in Statistical Physics* (Cambridge University Press, Cambridge, 1996).
[15] D. Stauffer and A. Aharony, *Introduction to Percolation Theory* (Taylor & Francis, London, 1992).
[16] M. E. J. Newman, Contemporary Physics **46**, 323 (2005).
[17] A. A. Middleton and D. S. Fisher, Phys. Rev. B **65**, 134411 (2002).
[18] O. Perković, K. Dahmen, and J. P. Sethna, Phys. Rev. Lett. **75**, 4528 (1995).
[19] Y.-J. Chen, S. Papanikolaou, J. P. Sethna, S. Zapperi, and G. Durin, Phys. Rev. E **84**, 061103 (2011).
[20] See Supplemental Material at [URL will be inserted by publisher], which includes Refs. [40–50].
[21] A. Coniglio, C. R. Nappi, F. Peruggi, and L. Russo, J. Phys. A **10**, 205 (1977).
[22] P. E. Berche, C. Chatelain, B. Berche, and W. Janke, Eur. Phys. J. B **38**, 463 (2004).
[23] V. S. Dotsenko, M. Picco, P. Windey, G. Harris, E. Martinec, and E. Marinari, Nucl. Phys. B **448**, 577 (1995).
[24] E. T. Seppälä, V. Petäjä, and M. J. Alava, Phys. Rev. E **58**, R5217 (1998).
[25] J. L. Cambier and M. Nauenberg, Phys. Rev. B **34**, 8071 (1986).
[26] D. A. Huse and S. Leibler, J. Phys. France **49**, 605 (1988).
[27] Y. Liu and K. A. Dahmen, Phys. Rev. E **79**, 061124 (2009).
[28] Y. Liu and K. A. Dahmen, Europhys. Lett. **86**, 56003 (2009).
[29] C. Frontera and E. Vives, Phys. Rev. E **62**, 7470 (2000).
[30] A. Frenzel, M. M. Qazilbash, M. Brehm, B.-G. Chae, B.-J. Kim, H.-T. Kim, A. V. Balatsky, F. Keilmann, and D. N. Basov, Phys. Rev. B **80**, 115115 (2009).
[31] J. P. Sethna, K. A. Dahmen, and C. R. Myers, Nature **410**, 242 (2001).
[32] J. P. Sethna, K. Dahmen, S. Kartha, J. A. Krumhansl, B. W. Roberts, and J. D. Shore, Phys. Rev. Lett. **70**, 3347 (1993).
[33] A. A. Middleton, Phys. Rev. Lett. **68**, 670 (1992).
[34] M. M. Qazilbash, M. Brehm, G. O. Andreev, A. Frenzel, P.-C. Ho, B.-G. Chae, B.-J. Kim, S. J. Yun, H.-T. Kim, A. V. Balatsky, O. G. Shpyrko, M. B. Maple, F. Keilmann, and D. N. Basov, Phys. Rev. B **79**, 075107 (2009).
[35] S. Kumar, M. D. Pickett, J. P. Strachan, G. Gibson, Y. Nishi, and R. S. Williams, Adv. Mater. **25**, 6128 (2013).
[36] K. Binder, J. Phys. Colloques **41**, C4 (1980).
[37] D. S. Fisher, Phys. Rev. Lett. **56**, 416 (1986).
[38] Y. Kohsaka, C. Taylor, K. Fujita, A. Schmidt, C. Lupien, T. Hanaguri, M. Azuma, M. Takano, H. Eisaki, H. Takagi, S. Uchida, and J. C. Davis, Science **315**, 1380 (2007).
[39] A. Moreo, M. Mayr, A. Feiguin, S. Yunoki, and E. Dagotto, Phys. Rev. Lett. **84**, 5568 (2000).
[40] W. Janke and A. M. J. Schakel, Phys. Rev. E **71**, 036703 (2005).
[41] D. Stauffer, Phys. Rep. **54**, 1 (1979).
[42] T. Grossman and A. Aharony, J. Phys. A **19**, L745 (1986).
[43] A. J. Bray and M. A. Moore, J. Phys. C **18**, L927 (1985).
[44] E. Seppälä, *Ground State Structure, Domain Walls, and External Field Response in Random Magnets*, Ph.D. thesis, Department of Engineering Physics and Mathematics, Helsinki University of Technology (2001).
[45] R. Guida and J. Zinn-Justin, J. Phys. A **31**, 8103 (1998).
[46] C. D. Lorenz and R. M. Ziff, Phys. Rev. E **57**, 230 (1998).
[47] R. M. Bradley, P. N. Strenski, and J.-M. Debierre, Phys. Rev. B **44**, 76 (1991).
[48] B. G. Chae, H. T. Kim, S. J. Yun, B. J. Kim, Y. W. Lee,

D. H. Youn, and K. Y. Kang, Electrochem. Solid-State Lett. **9**, C12 (2006).
[49] E. U. Donev, R. Lopez, L. C. Feldman, and R. F. Haglund, Nano Letters **9**, 702 (2009).
[50] M. K. Liu, M. Wagner, E. Abreu, S. Kittiwatanakul, A. McLeod, Z. Fei, M. Goldflam, S. Dai, M. M. Fogler, J. Lu, S. A. Wolf, R. D. Averitt, and D. N. Basov, Phys. Rev. Lett. **111**, 096602 (2013).